Critical behavior of a fully frustrated classical XY model in two dimensions

Julio F. Fernández*
Instituto Venezolano de Investigaciones Científicas (IVIC), Apartado 21827, Caracas 1020-A, Venezuela

Marcello Puma†
Centro Científico, IBM, Caracas, Venezuela

Rafael F. Angulo
INTEVEP, Investigación básica, Apartado 70363, Caracas 1070A, Venezuela
(Received 26 November 1990; revised manuscript received 24 June 1991)

We simulate, by the Monte Carlo method, a fully frustrated antiferromagnet of classical XY spins on a square lattice in two dimensions, with nearest- and second-nearest-neighbor interactions (J_1 and J_2) for $J_1=J_2$. Rotations of all spins on one sublattice with respect to all spins on the other sublattice leave the *ground-state* energy invariant. We first check, numerically, that the temperature does, as previously predicted, introduce an anisotropy that gives rise to an Ising-like broken symmetry in the ordered state at $T>0$. Our results are consistent with one critical temperature, where both magnetization fluctuations and fluctuations of the appropriate Ising-like order parameter diverge. Critical fluctuations of the magnetization seem to cross over from a Kosterlitz-Thouless-type behavior to $\xi\sim t^{-\nu}$ ($\nu\approx 1$) as ξ becomes large enough ($\xi>10$ lattice units) for anisotropy effects to become dominant. Values of several critical indices are obtained. In addition, critical effects produced by small amounts of impurities are studied. We find that the reduced crossover temperature into the impurity-dominated regime is given by $t\sim\delta n^{2/\phi},\phi\approx 1.7$, where δn is the impurity concentration. This result differs sharply from the predictions of the Harris criterion.

I. INTRODUCTION

There has been some recent interest in frustrated systems of classical planar spins (XY model) in two-dimensional (2D) lattices.[1] Some of it has arisen out of the possible connection between magnetism and high-temperature superconductivity.[2] Villain's[3] odd model: a system with ferromagnetic nearest-neighbor exchange interactions everywhere on a square lattice except for every other row (or column) where the exchange bonds are antiferromagnetic, provides an example of a fully frustrated XY (FFXY) model. It corresponds to an array of Josephson junctions with an applied magnetic field.[4] The *antiferromagnetic* XY model on a triangular lattice, another version of a FFXY model, has also been studied.[5]

The critical behavior of FFXY models is not expected to belong to the Kosterlitz-Thouless (KT) universality class because more symmetries of the Hamiltonian are broken in the ground state of FFXY models than in the ground state of XY ferromagnets. Consider the model Hamiltonian we study here:

$$H=+J_1\sum_{\langle ij\rangle}\mathbf{S}_i\cdot\mathbf{S}_j+J_2\sum_{\langle\mu\nu\rangle}\mathbf{S}_\mu\cdot\mathbf{S}_\nu\ , \tag{1}$$

where the sums are over all ij and all $\mu\nu$, first- and second-nearest-neighbor pairs of sites on a square lattice, respectively, s_i is a two-component unit vector on site i, and $J_2>|J_1/2|$. (We will refer to this fully frustrated next-nearest-neighbor XY model as the FFNNXY model.) The ground state is pictured in Fig. 1(a); it is easily seen that its energy is independent of θ, but, as Henley[6] has shown, there is an anisotropy for nonvanishing temperatures: spins on one sublattice [see Fig. 1(a)] tend to be either parallel or antiparallel to spins on the other sublattice. A reflection of the lattice with respect to line DD in Fig. 1(a) leaves H invariant, but it transforms one ordered state into the other degenerate ordered state. These same two symmetries [Z_2 and U(1)] are involved in the transition of the other two FFXY systems mentioned above.[3,5] Ising- and KT-like transitions might consequently be expected at some temperatures T_I and T_{XY}, respectively. Most, but not all,[7] work done on the triangular antiferromagnet and on Villain's model gives $T_I=T_{XY}$.[3,5] Ising-like domains and XY vortices may very well interact giving rise to a universality class which remains to be established.[8] The critical behavior of the FFNNXY model has not, as far as we know, been explored.

We do Monte Carlo (MC) simulations (Metropolis algorithm) for systems of $L\times L$ spins for $L=20$, 30, 40, 60, 100, and 150 for different temperatures of the FFNNXY antiferromagnet with $J_2=J_1=1$. We find that, within the accuracy of our results, there is only one critical temperature, $T_c=(0.90\pm 0.02)$. There also seems to be only one critical correlation length ξ, both for magnetization fluctuations and for fluctuations of an appropriate Ising-like order parameter. The small anisotropy (which generates the Z_2 symmetry) in the model seems to drive the system away from a Kosterlitz-Thouless (KT) behavior when the correlation length becomes large enough. We determine the values of several critical indices.

The effect of some randomness on the critical behavior of the XY antiferromagnet on a triangular lattice and on the XY Villain model can be strong.[9] However, no work has been reported on the crossover behavior, from the pure regime behavior, far away from the critical point, into the impurity dominated regime near the critical point. We study it here for the FFNNXY model. On the basis of work done thus far on fully frustrated Ising models,[10] we expect it to be interesting because, in contrast with the case of ferromagnets, missing nearest-neighbor bonds (or missing pairs of nearest-neighbor spins) break the Z_2 symmetry in these systems. We find that the reduced crossover temperature is given by

$$t_c \sim \delta n^{2/\phi} , \tag{2}$$

where δn is the impurity concentration (e.g., fraction of missing bonds), and $\phi=\gamma_1$, which is radically different from the value of $\phi=\alpha$ (the so-called Harris criterion), where α is the specific heat exponent, which holds for the unfrustrated (e.g., ferromagnetic) XY model.

In order to state the plan and main results of the paper in greater detail we first define some quantities. Let

$$\Psi_i=[(\mathbf{s}_i-\mathbf{s}_j)/2]\cdot[(\mathbf{s}_k-\mathbf{s}_m)/2] , \tag{3}$$

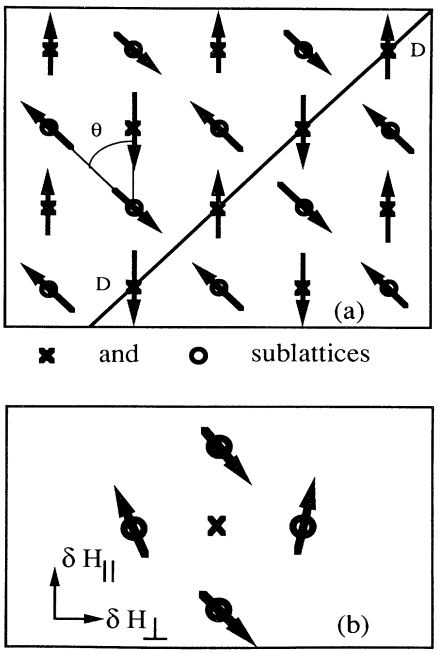

FIG. 1. A ground-state spin configuration is shown in (a). The circles denote sites on the A sublattice whereas the crosses are on sites on the B sublattice. The angle θ between spins on the two sublattice is shown. The Hamiltonian is invariant with respect to reflection about the DD axis. The ground state shown transforms into another degenerate state upon such a reflection. Four nearest neighbors to a spin (at the center) are shown in (b). The four spins deviate slightly from the ground-state configuration, and produce therefore a field $\delta H_\perp$ which is linear in the angle of deviation and a field $\delta H_\parallel$ quadratic in the angle of deviation.

where sites i, j, k, and m lie on the four corners of a plaquette, i diagonally across from j and k diagonally across from m. We assign the index i to Ψ to indicate which plaquette it is associated with. We further define

$$\chi_1=N^{-1}\sum_{i,j}\langle(\Psi_i-\langle\Psi_i\rangle)(\Psi_j-\langle\Psi_j\rangle)\rangle \tag{4}$$

and

$$S_2=\frac{2}{N}\left[\sum_{i,j\in A}\langle\tau_i\cdot\tau_j\rangle+\sum_{k,m\in B}\langle\tau_k\cdot\tau_m\rangle\right] , \tag{5}$$

where N is the total number of sites, $\tau_i=(-1)^{(X_i+Y_i)}s_i$, X_i and Y_i are the coordinates of site i (the nearest-neighbor distance is one unit of length), and the sum in Eq. (4) is over all i and j sites, whereas the first and second sums in Eq. (5) are only over all points on the A and B sublattices, respectively.

We next give the outline of the paper, and values found for the critical indices. Details about the MC runs are given on the first subsection in Sec. II. Monte Carlo results are shown in Sec. II B which support Henley's conclusion: that there is an Ising-type (Z_2) broken symmetry in the FFNNXY model at low T. Let $t=|T-T_c|/T_c$ and

$$\langle\Psi\rangle=N^{-1}\sum_i\langle\Psi_i\rangle . \tag{6}$$

Our MC results show that the transition temperature T_I, below which $\langle\Psi\rangle\neq 0$, and the transition temperature T_{XY}, where S_2 diverges, are equal within the accuracy (2%) of our results (shown in Sec. II C). The critical index values we have found, which we defined next, are given in Sec. III. We find for β, defined by $\langle\Psi\rangle\sim t^\beta$, a value of 0.15 ± 0.05. We have found $\gamma_1=1.6\pm0.2$ (γ_1 is defined by $\chi_1\sim t^{-\gamma_1}$). S_2 seems to diverge as $\chi_2\sim t^{-\gamma_2}$, and *not* as in a Kosterlitz-Thouless transition. This point is discussed in Sec. V. We find $\gamma_2=1.5\pm0.2$. We obtain for η_1, defined by

$$\langle(\Psi_i-\langle\Psi_i\rangle)(\Psi_j-\langle\Psi_j\rangle)\rangle\sim\{\exp[-r_{ij}/\xi_1(T)]\}/r_{ij}^{\eta_1} , \tag{7}$$

the value 0.4 ± 0.1. Assuming the same spatial dependence for $\langle\tau_i\tau_j\rangle$ one can similarly define ξ_2 and η_2. We obtain $\eta_2=0.35\pm0.08$. Section IV deals with the question of the effect of small amounts of impurities on the critical behavior. As expected, on the basis of work previously done on the Ising model, the effect is much stronger than that predicted by Harris for the ferromagnet. We show that $\phi=\gamma_1$. Our numerical results give $\phi=1.7\pm0.3$, in agreement, within the given errors, with the value found for γ_1.

II. MC RESULTS FOR ANISOTROPY AND CRITICAL TEMPERATURES

A. The Monte Carlo runs

We have done Monte Carlo runs on systems of $L\times L$ spins for $L=20$, 30, 40, 60, 100, and 150 for different

temperatures. All temperatures are given in units of $|J_2|/k_B$, where k_B is Boltzmann's constant. $3L^2$ sweeps to equilibrate and $20L^2$ sweeps in equilibrium were made in the neighborhood of the critical point (5×10^5 sweeps were done in equilibrium on systems of 150×150 spins). Runs were shorter away from the critical point: $3L\times L$ sweeps to equilibrate and $6L\times L$ sweeps in equilibrium. The number of sweeps goes like L^2 because the relaxation time increases as L^2 at the critical point. Most runs for $L\leq100$ were performed on a SUN sparc1 work station, but an IBM 3090 computer was used for $L=150$. 2×10^5 sweeps on a system of 100×100 spins took about 30 h of computer time on the SUN; 5×10^5 sweeps on a system of 150×150 spins took about 50 h on an IBM 3090.

Averages are computed as usual. In particular, $\langle\Psi\rangle$ is computed as the average of $|\Psi|$ over all states visited after equilibration is achieved.

B. Anisotropy

The purpose of this subsection is to exhibit the effect of the Ising-type (Z_2) broken symmetry in the FFNNXY model at low temperature. Collinearity of spins on different sublattices comes about, as Henley[6] first explained, at $T\neq0$ as spins try to follow the thermal fluctuations of their nearest neighbors. Consider the nearest neighbors to a given spin. Small independent random angular deviations ($\sim\delta\theta$) from their average directions produce an effective field on the spin considered with components $\delta H_\perp\sim\delta\theta$ and $\delta H_\parallel\sim\delta\theta^2$ [see Fig. 1(b)]. Being initially nearly collinear (perpendicular) to its neighbors, a spin can lower its energy by $\sim\delta\theta^2(\delta\theta^3)$, by adjusting its direction by $\delta\theta$. Henley[6] has obtained, for $k_BT/|J_2|\ll1$,

$$\Delta f(\theta)\cong0.08T(J_1/J_2)^2(1-\cos^2\theta) \quad (8)$$

for the free energy (per spin) variation with θ. In order to check this equation we have obtained histograms of the number of times $n(\theta)$ that θ takes a given value in a MC run of a 40×40 spin system in equilibrium. Since the probability density $P(\theta)$ that takes a given value fulfills, $P(\theta)\propto\exp[-\Delta f(\theta)N/T]$, it follows that a plot of $\ln[n(\theta)/N]$ versus θ^2 should give $-\Delta f(\theta)/T$ up to a constant. Figure 2 shows the data points obtained for $\Delta f(\theta)/T$ (up to a constant). Both small T and θ^2 dependences check out reasonably well [there is only a minor discrepancy: the coefficient of Eq. (8) seems to be a factor of about 2 too large].

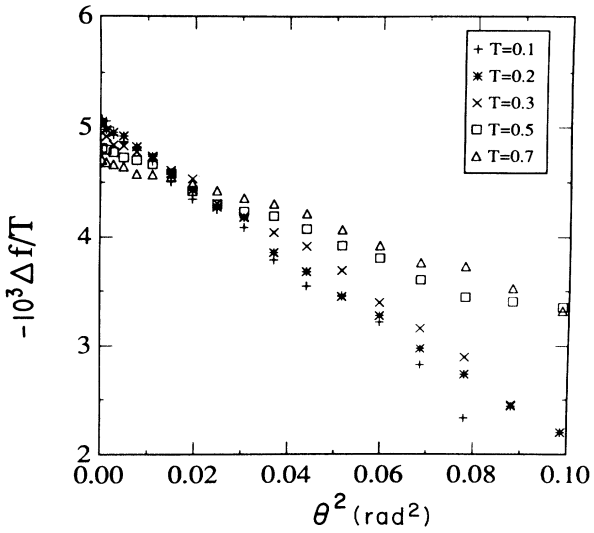

FIG. 2. Quantity $-\Delta f/T$ (up to a constant) is shown as a function of θ^2, where f is the free energy and θ is the angle shown in Fig. 1. The θ and T dependence shown in Eq. (8) seem to be satisfied for small T. Error bars are about the size of the data point symbols shown.

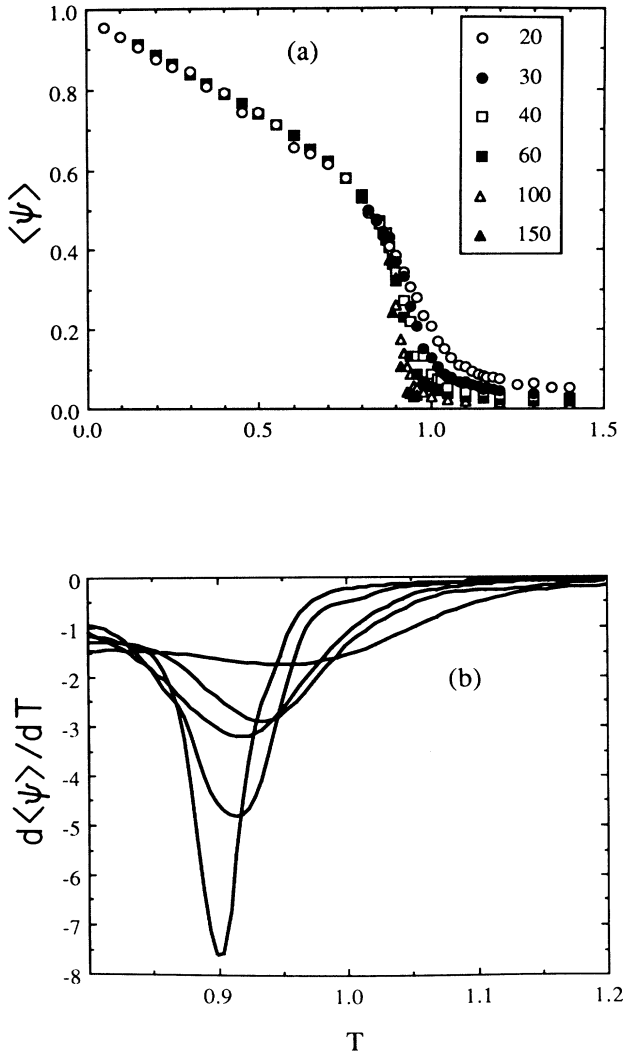

FIG. 3. (a) The order parameter defined in Eqs. (3) and (6) is shown for systems for various sizes as functions of T. Error bars are about the size of the data point symbols shown. (b) The slope of $\langle\Psi\rangle$ vs T, obtained from cubic spline fits to the curves shown in (b), is shown.

C. Critical temperatures

We next estimate T_I, the temperature below which $\langle\Psi\rangle\neq 0$, $\langle\Psi\rangle$, and $d\langle\Psi\rangle/dT$ are shown in Figs. 3(a) and 3(b), respectively, for systems of various sizes as functions of T. We estimate T_I as follows: let $T_I(\Psi,L)$ be defined by $d^2\langle\Psi\rangle/dT^2=0$ for a system of $L\times L$ spins, that is by the point where the order parameter decreases fastest; the limit of $T_I(\Psi,L)$ as $1/L\to 0$ yields T_I. In order to estimate the error involved we define similarly $T_I(S_1,L)$ and $T_I[\log_{10}(S_1),L]$, by the location of the maxima of dS_1/dT and of $d\log_{10}(S_1)/dT$ where $S_1=N^{-1}\sum\langle\Psi_i\Psi_j\rangle$. The results are exhibited in Fig. 4. Figure 5 shows the susceptibility-like quantity, χ_1 for systems of various sizes. From the data shown in Figs. 4 and 5, we conclude that $T_I=0.89\pm 0.01$.

We follow a similar procedure to estimate the value of T_{XY}, except that a nonvanishing order parameter does not exist in this case. We define values of T_{XY} (L) by the location of maxima of dS_2/dT and of $d[\log_{10}(S_2)]/dT$. These values and their $1/L\to 0$ extrapolation are also shown in Fig. 4. Inspection of that figure shows that $|T_{XY}-T_I|$ is not larger than the errors of either T_{XY} or T_I. We conclude that

$$T_I\cong T_{XY}=0.90\pm 0.02\ . \tag{9}$$

We will make no distinction between T_I and T_{XY} from here on and will just refer to either one as T_c.

III. CRITICAL INDICES

A. Order parameter

The order parameter $\langle\Psi\rangle$ is shown in Fig. 3 as a function of T. In order to exhibit the critical behavior, $\langle\Psi\rangle\sim t^{-\beta}$, data $\log_{10}(\langle\Psi\rangle)$ versus $\log_{10}(T_c-T)$ are shown in Fig. 6 for various values of L, using $T_c=0.9$. The best straight-line fit to the data in the range $0.82\le T\le 0.89$ gives $\beta=0.15$. Statistical errors in the values of $\langle\Psi\rangle$ lead to an error of about 0.03. Using the smallest or largest values allowed for T_c, 0.88 and 0.92, respectively, one obtains plots which deviate very markedly from straight-line behavior. Even the values $T_c=0.89$ or $T_c=0.91$ lead to appreciable deviations. Variations of T_c within the 0.89 to 0.91 range give an error of about 0.04 in the value of β. Adding these two errors incoherently, we obtain

$$\beta=0.15\pm 0.05\ . \tag{10}$$

B. Susceptibilities

The critical behavior of the susceptibility-like quantity χ_1, defined in Eq. (4), and exhibited in Fig. 5 is examined next. It follows from Eqs. (4) and (7) that

$$\chi_1\sim\xi_1^{(2-\eta_1)}\ . \tag{11}$$

We first try $\xi_1\sim t^{-\nu_1}$. Then

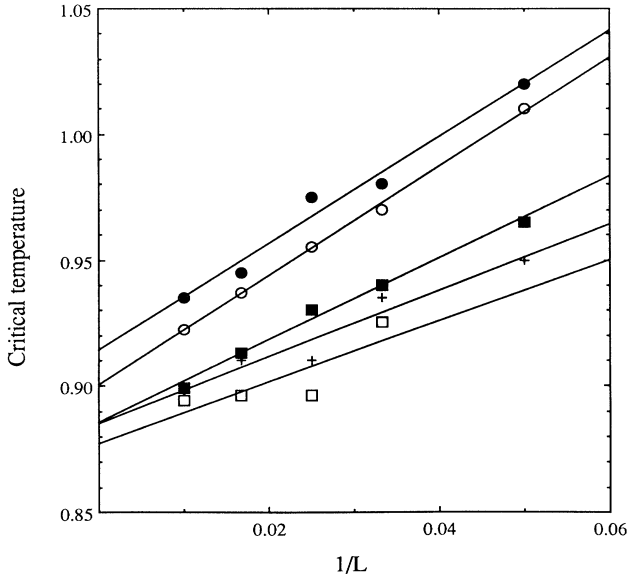

FIG. 4. The purpose of this figure is to exhibit how the critical temperatures T_I and T_{XY} are estimated. Values of T where the maxima of $d\langle\Psi\rangle/dT$ occur are plotted versus $1/L$ as crosses (+); similarly (□) for $d\chi_1/dT$, (○) for $d[\log_{10}(\chi_1)]/dT$, (■) for dS_2/dT and (○) for $d[\log_{10}(S_2)]/dT$. Extrapolations to $1/L\to 0$ give the corresponding estimates of T_I and of T_{XY}.

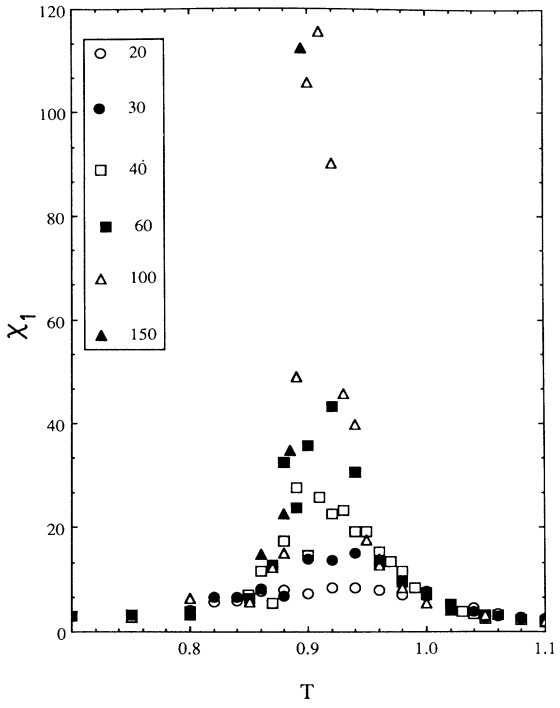

FIG. 5. Data points are shown for χ_1 as a function of temperature for systems of $L\times L$ spins. The corresponding values of L are shown in the upper left-hand corner.

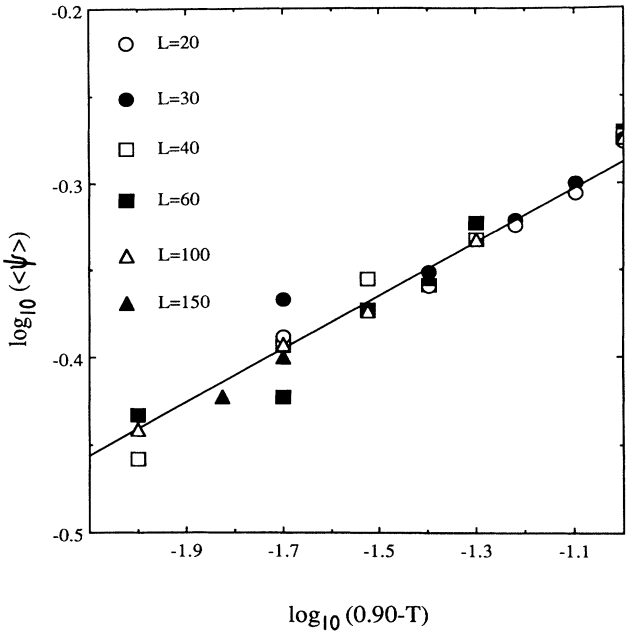

FIG. 6. Data points are shown for the logarithm of the order parameter $\langle\Psi\rangle$ as a function of the logarithm of $(0.9-T)$ for systems of $L\times L$ spins (0.9 is the value we have found for T_I). The corresponding values of the L are shown in the upper left-hand corner. The slope of the straight line shown gives $\beta=0.15$. Error bars are in agreement with the scatter in the data.

$$\chi_1 \sim t^{-\gamma_1} , \tag{12}$$

where $\gamma_1=\nu_1(2-\eta_1)$. A plot of $\log_{10}(\chi_1)$ versus $\log_{10}|T-0.9|$ of the data is shown in Fig. 7. Not much can be inferred from the data below T_c (inset) as the critical region seems to be rather narrow there. A straight-line fit to all the data points shown which are seemingly free of finite-size effects above T_c gives $\gamma_1\approx 1.6$. Statistical errors in the data give an error of 0.1 at most. On the other hand, using the smallest or largest values allowed for T_c, 0.88 and 0.92, respectively, one obtains plots which deviate quite markedly from straight-line behavior. Even the value $T_c=0.89$ or $T_c=0.91$ lead to appreciable deviations. Variations of T_c within the 0.89 to 0.91 range give an error of about 0.15 in the value of γ_1. Adding these two errors incoherently, we obtain

$$\gamma_1=1.6\pm 0.2 . \tag{13}$$

We now try the Kosterlitz-Thouless expression $\xi_1\sim\exp(b/t^{\nu_1})$. Equation (11) then becomes $\chi_1\sim\exp(b'/t^{\nu_1})$. Figure 8 shows a plot of $\log_{10}[\log_{10}(\chi_1)]$ versus $\log_{10}|T-0.9|$. The data points depart significantly from a straight line. This result is fairly independent of the value of T_c chosen. The inset in Fig. 8, which shows a plot of $\log_{10}[\log_{10}(\chi_1)]$ versus $\log_{10}|T-T_c|$, for $T_c=0.89$, illustrates the point.

The critical behavior of the structure factor S_2, defined in Eq. (5), is examined next. Since $\langle s_i\rangle=0$, S_2 is a susceptibility. If we assume $\xi_2\sim t^{-\nu_2}$, then $S_2\sim\xi_2^{(2-\eta_2)}$ leads us to $S_2\sim t^{-\gamma_2}$. Figure 9 exhibits the critical behavior of S_2. Proceeding as for χ_1, we obtain

$$\gamma_2=1.5\pm 0.2 . \tag{14}$$

Again, we try the KT expression $\xi_2\sim\exp(b/t^{\nu_2})$. Then, $S_2\sim\exp(b'/t^{\nu_2})$. Figure 10 shows a plot of $\log_{10}[\log_{10}(S_2)]$ versus $\log_{10}|T-0.9|$. The data points also depart significantly from a straight line in this case; this result is again fairly independent of the value of T_c chosen. This result is discussed in Sec. V.

Equation (11) becomes for finite systems, according to finite-size scaling,[12]

$$\chi_1\sim\xi_1^{(2-\eta_1)} f(\xi_1/L) , \tag{15}$$

where f is some function. $\chi_1\rightarrow L^{2-\eta_1}$ as $T\rightarrow T_c$. Figure 11 shows our results in a $\log_{10}(\chi_1)$ versus $\log_{10}(L)$ for various values of T. The best straight-line fit to the $T=0.9$ data points gives $2-\eta_1=1.57$. Inspection of the figure shows that the error in $2-\eta_1$ is about 0.1. Therefore,

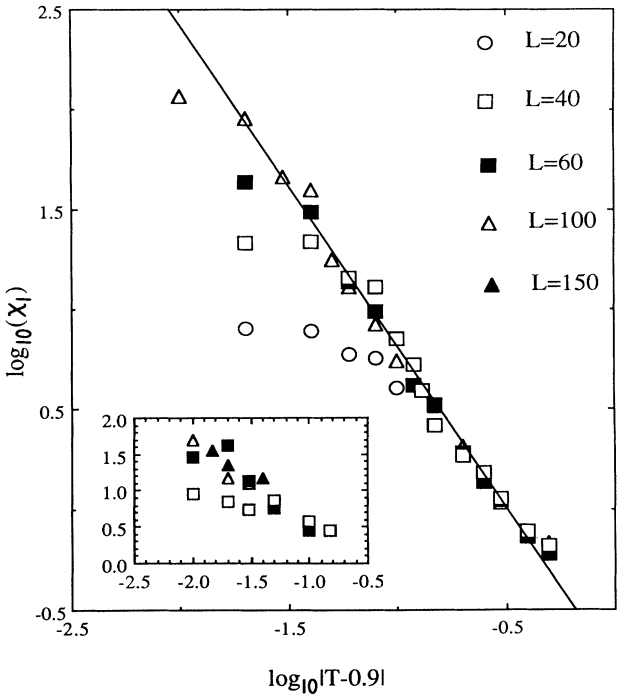

FIG. 7. Data points are shown for the logarithm of χ_1, defined in Eq. (4) as a function of the logarithm of $|T-0.9|$ for systems of $L\times L$ spins (0.9 is the value we have found both for T_I and for T_{XY}). The corresponding values of L are shown in the upper right-hand corner. Error bars are about twice the size of the data point symbols shown. The inset shows $\log_{10}(\chi_1)$ vs $\log_{10}|0.9-T|$ for $T<T_I$. The slope of the straight line gives $\gamma_1=1.60$.

$$2-\eta_1=1.6\pm0.1\ . \tag{16}$$

We proceed similarly for S_2. The data is shown in Fig. 12. We obtain

$$2-\eta_2=1.65\pm0.08\ , \tag{17}$$

at the critical point ($T=0.9$).

Equations (13) and (14) plus Eqs. (16) and (17) together with $\gamma/\nu=2-\eta$ give $\nu_1=0.9\pm0.2$ and $\nu_2=1.0\pm0.2$.

C. Specific heat

Figure 13 shows our results for the energy $\langle E\rangle$ versus T, near T_c, for systems of various sizes. We have obtained the specific heat C by fitting $\langle E\rangle$ versus T, for each system size, with cubic splines, and then taking their derivatives. Now, from finite-size scaling,[12] $C\sim L^{\alpha/\nu}f(\xi/L)$, whence it follows that $C(T=T_c)\sim L^{\alpha/\nu}$. Figure 14 exhibits $C(T=T_c)$ versus $\log_{10}(L)$. One might be tempted to infer that C diverges at T_c on

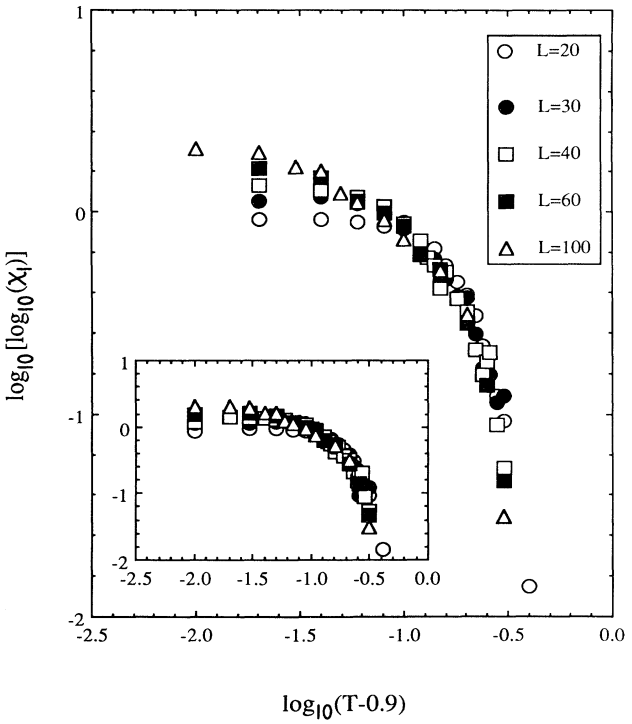

FIG. 8. The purpose of this figure is to contrast our results with the Kosterlitz-Thouless-like behavior, $\chi_1\sim\exp(b/t^{\nu})$. Data points are shown for the double logarithm of χ_1, defined in Eq. (4), as a function of the logarithm of $(T-0.9)$ for system of $L\times L$ spins (0.9 is the value we have found for T_I). The corresponding values of L are shown in the upper right-hand corner. The departure from straight-line behavior is fairly independent of the value one chooses for the transition temperature T_I; the inset illustrates the point: it shows a plot of $\log_{10}[\log_{10}(\chi_1)]$ vs $\log_{10}|T-T_I|$, for $T_I=0.89$. Error bars are about the size of the data point symbols shown.

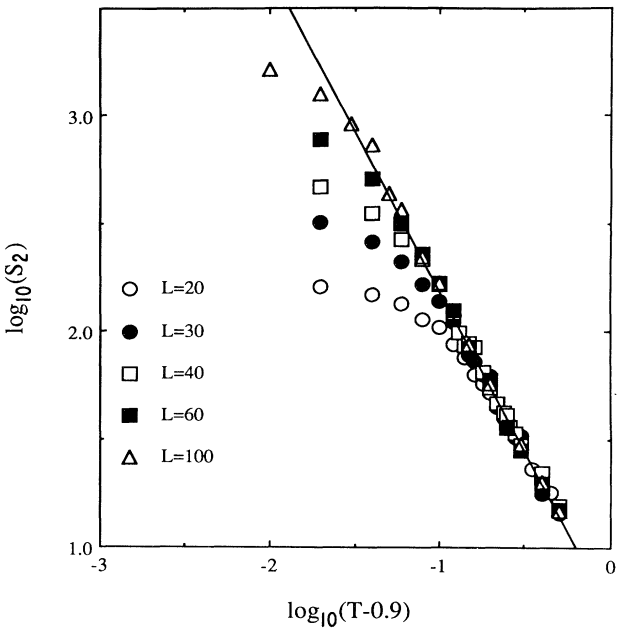

FIG. 9. Data points are shown for the logarithm of S_2, defined in Eq. (5) as a function of the logarithm of $(T-0.9)$ for systems of $L\times L$ spins (0.9 is the value we have found both for T_I and for T_{XY}). The corresponding values of L are shown in the lower left-hand corner. Error bars are about the size of the data point symbols shown. The slope of the straight line shown gives $\gamma_2=1.49$.

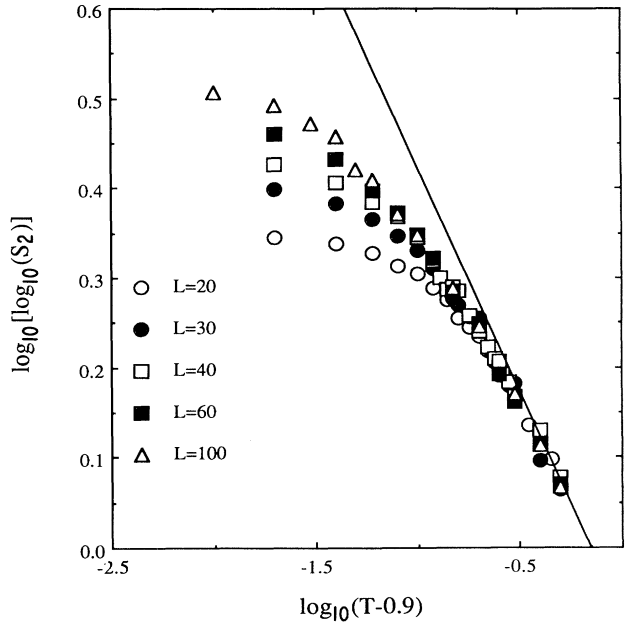

FIG. 10. The purpose of this figure is to contrast our results with the Kosterlitz-Thouless-like behavior, $S_2\sim\exp(b/t^{\nu})$. The straight line shown corresponds to $\nu=\frac{1}{2}$. Data points are shown for the double logarithm of S_2, defined in Eq. (5), as a function of the logarithm of $(T-0.9)$ for systems of $L\times L$ spins (0.9 is the value we have found for T_{XY}). The corresponding values of L are shown in the lower left-hand corner. Error bars are about the size of the data point symbols shown.

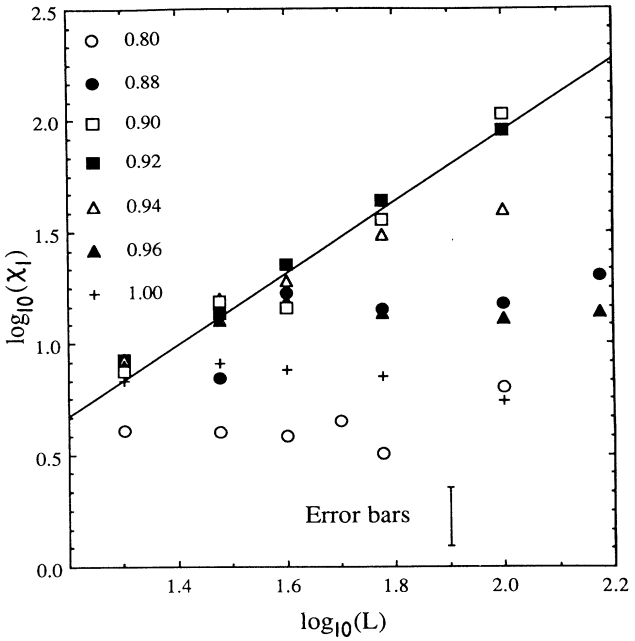

FIG. 11. Data points are shown for the logarithm of χ_1, defined in Eq. (4), as a function of the logarithm of L for the values of temperature shown at the upper left-hand corner. χ_1 diverges only at $T_l \approx 0.90$. The line is the best straight line fit to the $T=0.90$ data points. Its slope gives $\gamma_1/\nu = 1.60$.

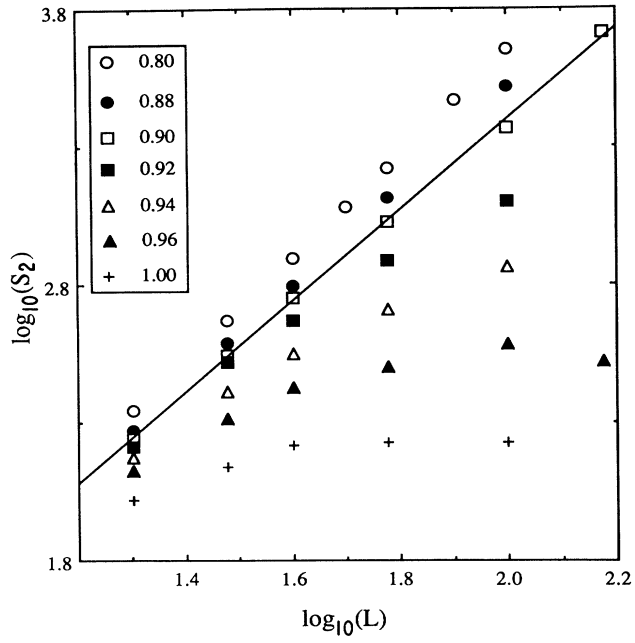

FIG. 12. Data points are shown for the logarithm of S_2, defined in Eq. (5), as a function of the logarithm of L for the values of temperature shown at the upper left-hand corner. Error bars are about the size of the data point symbols shown. The line is the best straight-line fit to the $T=0.90$ data points. Its slope gives $\gamma_2/\nu = 1.65$.

that basis. However, it also follows from finite-size scaling that $C_{\max} \sim L^{\alpha/\nu}$, where $C_{\max}$ is the maximum value of C versus T for each value of L [it follows from setting $dC/dt=0$, which implies $df(u)/du=0$, which in turn implies $\xi/L=\text{const}$, whence follows that $C_{\max} \sim L^{\alpha/\nu} f(\text{const})$]. Figure 14 also exhibits $C_{\max}$ versus $\log_{10}(L)$. It is not clear whether there is a divergence or not. Results for larger systems would help to resolve this point. (Note however that computing times increases as L^4, since the number of Monte Carlo steps *per spin* must increase as L^2 in the critical region.)

IV. CROSSOVER TO IMPURITY DOMINATED CRITICAL BEHAVIOR

This section is devoted to the effect of small amounts of impurities on the critical behavior. Our purpose is limited to establish the size of the neighborhood $|T_{cr}-T_c|$ next to the critical point where impurities dominate critical behavior. Our result is summarized by Eq. (2), where $t_c=|T_{cr}-T_c|/T_c$. To arrive at that result we do not simulate systems with impurities, rather, we extract our conclusions from the behavior of pure systems by the

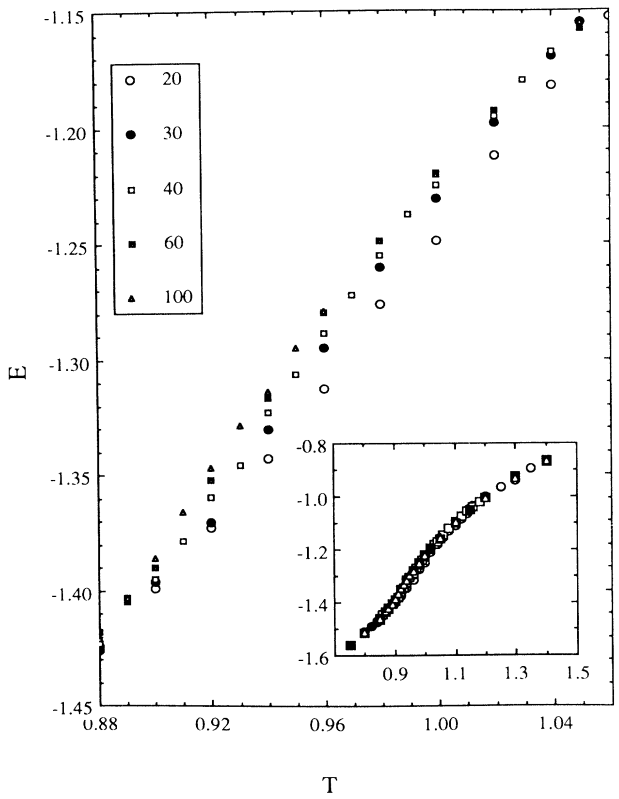

FIG. 13. Data points are shown for the mean energy per spin as a function of temperature for systems of $L \times L$ spins for the values of L shown at the upper left-hand corner. Error bars are about the size of the data point symbols shown. The inset shows the same quantity over a wider temperature range.

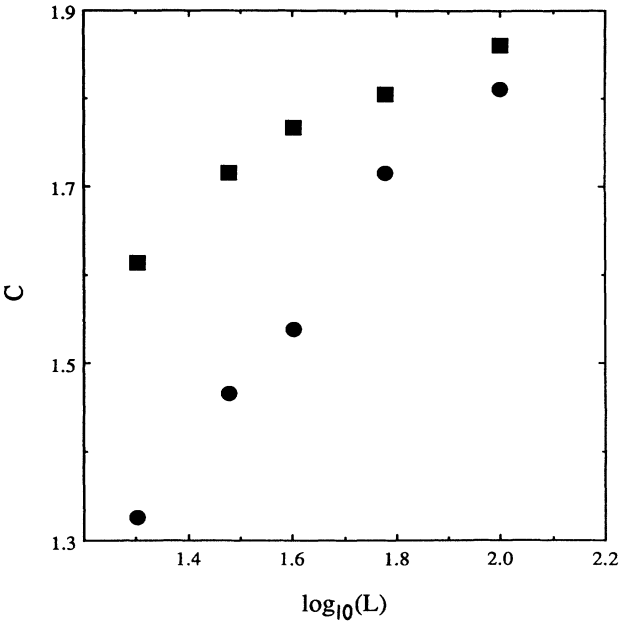

FIG. 14. Data points ● and ■ stand for the specific heat per spin at the critical temperature and its maximum value, respectively, as a function of the logarithm of L. The data points were obtained by taking derivatives of cubic spline fits of the curves shown in Fig. 13. Error bars are slightly larger than the size of the data point symbols shown.

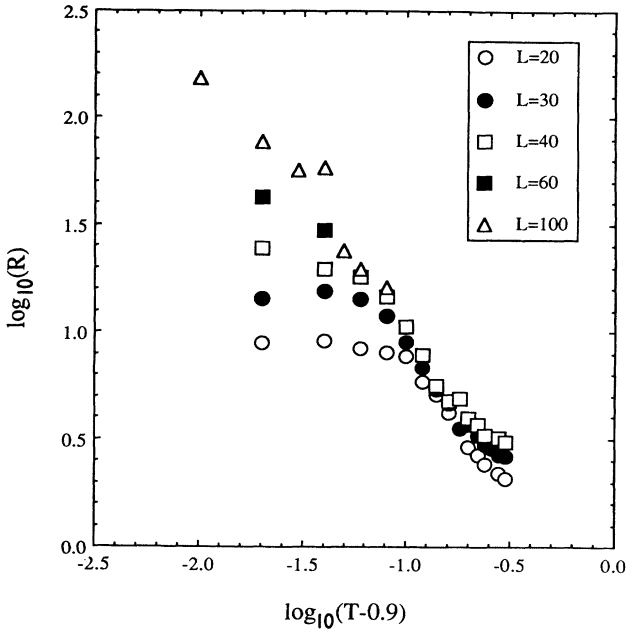

FIG. 15. Data points are shown for the logarithm of R, defined in Eq. (23) as a function of the logarithm of $(T-0.9)$ for systems of $L\times L$ spins (0.9 is the value we have found both for T_I and for T_{XY}). The corresponding values of L are shown in the upper right-hand corner. Error bars are slightly larger than the size of the data point symbols shown.

procedure described next.

Following Ref. 10 we let

$$H\rightarrow H+\sum_{i,j}\delta J_{ij}\mathbf{S}_i\cdot\mathbf{S}_j\ , \tag{18}$$

where H is the Hamiltonian for the pure system, the sum is over all nearest-neighbor pairs ij, and δJ_{ij} is an independent random variable. For simplicity's sake we will only consider nearest-neighbor bond impurities, that is, $\delta J_{ij}\neq 0$ only if i and j are nearest neighbors. Furthermore, $\langle\delta J_{ij}\rangle=0$ and $\langle\delta J_{ij}\delta J_{km}\rangle=\delta J^2(\delta_{ik}\delta_{jm}+\delta_{im}\delta_{jk})$. A cumulant expansion of the free energy gives

$$-\beta F=-\beta F_0+\beta^2(\delta J^2/2)\sum_{i,j}[\langle(\mathbf{S}_i\cdot\mathbf{S}_j)^2\rangle-\langle(\mathbf{S}_i\cdot\mathbf{S}_j)\rangle^2]\ , \tag{19}$$

to order δJ^2, where the sum is over all nearest-neighbor pairs. On the other hand, assuming scaling,[12]

$$F\sim t^{2-\alpha}f(\delta J^2/t\phi)\ , \tag{20}$$

where f is some function. Then, expanding to order δJ^2

$$F\sim t^{2-\alpha}[f(0)+f'(0)\delta J^2/t\phi]\ . \tag{21}$$

Comparing Eqs. (19) and (21) one gets

$$t^{2-\alpha-\phi}\sim\langle(\mathbf{S}_i\cdot\mathbf{S}_j)^2\rangle-\langle\mathbf{S}_i\cdot\mathbf{S}_j\rangle^2\ , \tag{22}$$

where i and j are nearest neighbors. We next examine the critical behavior of the second term which is the most singular one of the two. $\langle S_iS_j\rangle$ is a sum of the order parameter $\langle\Psi\rangle$ and the energy corresponding to nearest-neighbor bonds only, as follows from the definition of $\langle\Psi\rangle$ and from the homogeneity of the pure system. It follows then that $2-\alpha-\phi=2\beta$, since Ψ diverges more strongly than the energy. If one lets the perturbing term in Eq. (18) be $\delta h\sum_i\Psi_i$, one gets, proceeding along similar lines as above, the familiar scaling relation $2-\alpha-\gamma=2\beta$. It follows then that $\phi=\gamma_1$.

The relation $\phi=\gamma_1$ can be checked numerically as follows. Let

$$R=N^{-1}\left[\left\langle\sum_i(\mathbf{S}_i\cdot\mathbf{S}_j)^2\right\rangle-\left[\sum_i\langle\mathbf{S}_i\cdot\mathbf{S}_j\rangle\right]^2\right]\ , \tag{23}$$

where the sum is only over all sites i (but not over j), and j is any first nearest neighbor to i. As shown in Ref. 10, $R\sim t^{\phi}$. Figure 15 shows $\log_{10}(R)$ versus $\log_{10}(T-0.9)$ for systems of various sizes. Proceeding as for γ_1 and for γ_2, α value of $\phi=1.7\pm0.3$ is obtained, which agrees as predicted, within the given errors, with the value obtained for γ_1 in Sec. III.

V. DISCUSSION

We have obtained the values of the critical exponents, β, γ_1, γ_2, η_1, and η_2 for the fully frustrated next and next-nearest neighbor XY antiferromagnet. Our results for the specific heat are inconclusive. It is not clear whether it diverges or not.

The thermally induced anisotropy seems to drive the

FFNNXY system away from a KT-like critical behavior for $t \lesssim 0.1$. However, a straight-line fit to the data points shown in Fig. 10 for $t \gtrsim 0.1$ gives a slope of 0.5 approximately (in accordance with a KT-like behavior). That fits with the following picture. The anisotropy is small in this system; it can therefore become truly effective only over long distances, driving the system away from KT behavior only for long enough correlation lengths. More quantitatively, consider low temperatures where Eq. (8) holds for the anisotropy. Then, walls between domains are about $10/\sqrt{T}$ wide. For shorter distances, anisotropy effects are small. We therefore expect anisotropy effects to become important only for $\xi \gtrsim 10$ in the critical region (where $T \sim 1$). Figures 7–10 exhibit finite-size effects and can therefore be used to estimate $\xi(t)$. Indeed, we find $\xi \gtrsim 10$ for $t \lesssim 0.1$, in accordance with this picture.

ACKNOWLEDGMENTS

We are indebted to Professor J. Marro for helpful suggestions. One of us (J.F.F.) is grateful for the warm hospitality enjoyed when visiting the Applied Physics department at the University of Granada. We are grateful to IBM's Centro Científico in Caracas, where some of the computations were carried out, for their warm hospitality. We learned much about this system through discussions with Dr. C. L. Henley, and from Dr. J. Stankiewicz. J. Albarrán's computer work was of great help. Grants (No. S1-1914) from the Consejo Nacional de Investigaciones Científicas y Technológicas and (No. CI1 .0409.E) from the Commission of the European Communities were most helpful.

*Present address: Física Aplicada, Facultad de Ciencias, Universidad de Granada, 18071 Granada, Spain.

†Permanent address: Universidad Simón Bolívar, Apartado 89000, Caracas, Venezuela.

[1]See, for instance, M. Gabay, T. Garel, G. N. Parker, and W. M. Saslow, Phys. Rev. B **40**, 264 (1989).

[2]G. Deutscher and K. A. Müller, Phys. Rev. Lett. **59**, 1745 (1987); F. C Zhang and T. M. Rice, Phys. Rev. B **37**, 3759 (1988); J. Vannimenus, S. Kirkpatrick, F. D. M. Haldane, and C. Jayaprakash, *ibid.* **39**, 4634 (1989); P. Coleman, J. Magn. Magn. Mater. **82**, 159 (1989); P. Chandra, P. Coleman, and A. I. Larkin, Phys. Rev. Lett. **64**, 88 (1990); E. Dagotto, R. Joynt, A. Moreo, S.Bacci, and E. Gagliano, Phys. Rev. B **41**, 9049 (1990).

[3]J. Villain, J. Phys. C **10**, 1717 (1977); for MC results, see S. Teitel and C. Jayaprakash, Phys. Rev. B **22**, 598 (1983); B. Berge, H. T. Diep, A. Ghazali, and P. Lalleman, *ibid.* **34**, 3177 (1986); for renormalization group work, see, T. C. Hasley, J. Phys. C **18**, 2437 (1985); M. Yosefin and E. Domany, Phys. Rev. B **27**, 1778 (1985); M. Y. Choi and S. Doniach, *ibid.* **31**, 4516 (1985); E. Granato, J. Phys. C **20**, L215 (1987).

[4]For a review, see, for instance, C. Lobb, Physica B **152**, 1 (1988).

[5]For an introduction and mean-field treatment, see D. H. Lee, R. G. Caflish, J. D. Joannopolous, and F. Y. Wu, Phys. Rev. B **29**, 2680 (1984); for MC results, see D. H. Lee, J. D. Joannopolous, J. W. Negele, and D. P. Landau, *ibid.* **33**, 450 (1986); J. E. van Himbergen, *ibid.* **34**, 6567 (1986).

[6]C. L. Henley, Phys. Rev. Lett. **62**, 2056 (1989); C. L. Henley and S. Prakash, J. Phys. C **491**, 1197 (1988).

[7]A T_I slightly larger than T_{XY} was obtained by S. Miyashita and H. Shiba [J. Phys. Soc. Jpn. **53**, 1145 (1984)].

[8]See, for instance, E. Granato and J. M. Kosterlitz, Phys. Rev. B **33**, 4767 (1986), Refs. 3 and 5.

[9]J.M. Kosterlitz and E. Granato, Physica B **152**, 62 (1988); K. A. Benedict and M. A. Moore, Phys. Rev. B **39**, 4592 (1989); see also M. Y. Choi and D. Stroud, *ibid.* **35**, 1669 (1987); for experiments, M. G. Forrester, H. J. Lee, M. Tinkham, and C. J. Lobb, *ibid.* **37**, 5966 (1988).

[10]J. F. Fernández, Europhys. Lett. **5**, 129 (1988); Phys. Rev. B **36**, 6901 (1988).

[11]M. E. Fisher, Phys. Rev. **176**, 257 (1968); A. B. Harris, J. Phys. C **7**, 1671 (1974); D. Andelman and A. Aharony, Phys. Rev. B **31**, 4305 (1985); R. R. P. Singh and M. E. Fisher, J. Appl. Phys. **63**, 3082 (1988); for experimental work, see R. J. Birgeneau, R. A. Cowley, G. Shirane, H. Yoshizawa, D. P. Belanger, A. R. King, and V. Jaccarino, Phys. Rev. B **27**, 6747 (1983); O. H. Barret, *ibid.* **34**, 3513 (1986).

[12]M. P. Nightingale and H. W. Blote, Physica **104A**, 352 (1980); V. Privman and M. E. Fisher, Phys. Rev. B **30**, 322 (1984).